# Gold Nanoparticle-Decorated Keggin Ions/TiO 2 Photococatalyst for Improved Solar Light Photocatalysis

**ARTICLE** · JANUARY 2011

CITATIONS
11

READS
32

**5 AUTHORS**, INCLUDING:

Andrew Pearson
RMIT University
**20** PUBLICATIONS **269** CITATIONS
SEE PROFILE

Kourosh Kalantar-zadeh
RMIT University
**404** PUBLICATIONS **7,610** CITATIONS
SEE PROFILE

Suresh Bhargava
RMIT University
**431** PUBLICATIONS **3,683** CITATIONS
SEE PROFILE

Vipul Bansal
RMIT University
**150** PUBLICATIONS **3,192** CITATIONS
SEE PROFILE

Langmuir

ARTICLE

pubs.acs.org/Langmuir

# Gold Nanoparticle-Decorated Keggin Ions/$TiO_2$ Photococatalyst for Improved Solar Light Photocatalysis

Andrew Pearson,[†] Harit Jani,[§] Kourosh Kalantar-zadeh,[‡] Suresh K. Bhargava,[*,†] and Vipul Bansal[*,†]

[†]School of Applied Science and [‡]School of Electrical and Computer Engineering, RMIT University, GPO Box 2476 V, Melbourne, Victoria 3001, Australia

[§]CSIRO Earth Science & Resource Engineering, Kensington, WA, 6151 (Australia)

Supporting Information

**ABSTRACT:** We demonstrate a facile localized reduction approach to synthesizing a Au nanoparticle-decorated Keggin ion/$TiO_2$ photococatalyst for improved solar light photocatalysis application. This has been achieved by exploiting the ability of $TiO_2$-bound Keggin ions to act as a UV-switchable, highly localized reducing agent. Notably, the approach proposed here does not lead to contamination of the resultant cocatalyst with free metal nanoparticles during aqueous solution-based synthesis. The study shows that for Keggin ions (phosphotungstic acid, PTA), being photoactive molecules, the presence of both Au nanoparticles and PTA on the $TiO_2$ surface in a cocatalytic system can have a dramatic effect on increasing the photocatalytic performance of the composite system, as opposed to a $TiO_2$ surface directly decorated with metal nanoparticles without a sandwiched PTA layer. The remarkable increase in the photocatalytic performance of these materials toward the degradation of a model organic Congo red dye correlates to an increase of 2.7-fold over that of anatase $TiO_2$ after adding Au to it and 4.3-fold after introducing PTA along with Au to it. The generalized localized reduction approach to preparing $TiO_2$−PTA−Au cocatalysts reported here can be further extended to other similar systems, wherein a range of metal nanoparticles in the presence of different Keggin ions can be utilized. The composites reported here may have wide potential implications toward the degradation of organic species and solar cell applications.

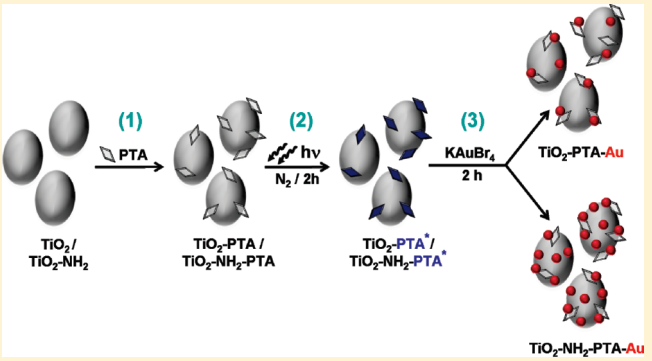


## INTRODUCTION

Titania ($TiO_2$) is a wide-band-gap semiconductor material that has received intense scrutiny for a broad range of applications, thanks to its intriguing physical−chemical properties and cheap, abundant, and reasonably nontoxic nature. $TiO_2$, also a widely used catalyst as well as a catalyst support,[1] is known to enhance the catalytic activity in many cases because of the strong interaction between the active phase and the support.[2] The photocatalytic properties of anatase $TiO_2$ in particular enjoy greater attention because of potential applications in paints and in the degradation of environmentally toxic dyes[3,4] and organic pollutants.[5,6] However, the application of $TiO_2$ particles is limited by the problems associated with the charge recombination (electron/hole recombination) phenomenon of semiconductor particles and also by their band-gap energy of 3.2 eV,[7] which typically requires exposure of ultraviolet light for $TiO_2$-mediated photocatalytic applications. As a result, for application purposes, a great deal of effort is ongoing to shift the band-gap energy of $TiO_2$ particles toward the visible region of the solar spectrum.[8−10] Additionally, various efforts have previously been made to dope small amounts of transition metals into the $TiO_2$ matrix to suppress the electron−hole recombination phenomenon.[11,12]

Both chemical and photodeposition methods are widely used for depositing noble metals on semiconductor nanoparticles, wherein the photoinduced deposition of noble metals such as Au and Pt on semiconductor nanomaterials has been previously employed to enhance their photocatalytic activity.[13−15] Recent efforts have also been made to bind metal nanoclusters to $TiO_2$ surfaces using a self-assembled monolayer approach.[16−19] Among various metal nanoparticles, the Au-$TiO_2$ system has received particular attention because of interesting phenomena occurring at the Au nanoparticle−$TiO_2$ matrix interface,[20] leading to demonstrated applications of Au−$TiO_2$ systems in nonlinear optical devices,[21−23] and photoelectrochemical solar cells.[7,24] Many other metal (M)−$TiO_2$ systems, such as V−$TiO_2$,[25] Pt−$TiO_2$,[26] Ni−$TiO_2$,[27] and Rh−$TiO_2$[28] have also been well studied. Similarly, Au-dispersed $TiO_2$ films have also been synthesized previously using different routes including RF sputtering[12,23] and liquid-phase deposition.[22] The most often used techniques for the preparation of $TiO_2$-supported metals are impregnation and ion

**Received:** February 28, 2011
**Revised:** April 13, 2011
**Published:** May 02, 2011

exchange,[29] which often require unfavorable conditions such as high temperatures and pressures. Additionally, in chemical routes of depositing metal nanoparticles onto a $TiO_2$ surface, the metal ion reduction step often leads to the formation of fresh metal nuclei in the solution, in addition to direct metal reduction on the $TiO_2$ surface. This is clearly undesirable from the application point of view because the final product contains a mixture of both metal nanoparticles and metal-decorated $TiO_2$ nanoparticles. A possible strategy to circumvent this drawback could be based on the immobilization of a reducing agent locally on the surface of $TiO_2$ particles, which when exposed to metal ions would reduce them, thereby leading to the formation of only metal-decorated $TiO_2$ nanoparticles without any free metal nanoparticles contamination.

To this end, although extensive research has been undertaken to develop metal-decorated $TiO_2$ nanoparticles, to the best of our knowledge limited or no studies have hitherto involved the use of a secondary photocatalytic linker molecule that when bound to the $TiO_2$ surface can also reduce metal ions specifically on its surface. In addition to facilitating the specific formation of metal−$TiO_2$ composites, these photocatalytically active molecules can also offer the additional advantage of enhancing the photocatalytic performance of the metal−photocatalytic linker−$TiO_2$ system.

Considering the aforementioned discussion, the incorporation of polyoxometallates (POMs) such as Keggin ions into $TiO_2$ is advantageous because they typically have high thermal stability[30] and can undergo stepwise multielectron redox processes without structural changes.[31] Additionally, Keggin ions can be easily reduced (electrolytically, photochemically, or with suitable reducing agents), and the reduced form of Keggin ions bound to $TiO_2$ can act as a reducing agent for metal ions[31] to decorate metal nanoparticles specifically on $TiO_2$ surfaces. Moreover, a vast range of Keggin ions are either commercially available or can be feasibly synthesized in laboratories, with applications in catalysis,[32,33] analytical chemistry,[34] electronics,[35] and medicine,[30] which pose them as promising molecules employable in the synthesis of advanced functional nanomaterials.[31,36] Papaconstantinou et al. demonstrated that the exposure of photochemically reduced silicotungstic acid $[(SiW_{12}O_{40})^{4-}]$ Keggin ions to aqueous metal ions resulted in the formation of a range of stable metal nanoparticles capped by Keggin ions.[37] Furthermore, Sastry et al. utilized phosphotungstic acid (PTA) $[(PW_{12}O_{40})^{3-}]$ Keggin ions bound to Au nanoparticle surfaces as localized reducing agents to form Au@Pt, Au@Pd, and Au@Ag core@shell nanoparticles.[31,36] Additionally, for catalysis applications, PTA is particularly promising because it is considered to be the strongest among the heteropolyacids, with an estimated acidity of the solid stronger than $-13.16(H_0)$, which means that PTA would qualify as a superacid and even at low pH PTA is fully dissociated.[37]

Because the photoexcitable reducing nature and catalytic properties of Keggin ions are well established, in this study we have, for the first time, utilized PTA bound to the $TiO_2$ surface as highly localized UV-switchable reducing agents to reduce Au nanoparticles specifically on the $TiO_2$ surface by a photoirradiation approach. Notably, with PTA being utilized as a localized reducing agent, our approach specifically leads to only Au-decorated $TiO_2$ particles in an aqueous-solution-based synthesis, without any contamination from free Au nanoparticles in solution via independent nucleation. We demonstrate that the loading of Au nanoparticles onto a $TiO_2$ surface can be feasibly fine tuned by controlling the $TiO_2$ surface charge by amine functionalization. The obtained $TiO_2$−PTA−Au and $TiO_2$−$NH_2$−PTA−Au composites have been characterized in detail using transmission electron microscopy (TEM), UV−visible, Fourier transform infrared (FTIR), and electron dispersive X-ray (EDX) spectroscopy, and X-ray diffraction (XRD), and their photocatalytic activity toward the degradation of model organic azo dye Congo red has been explored under simulated solar light conditions.

**Scheme 1. Schematic Representation of the Formation of the Au Nanoparticle-Decorated $TiO_2$−PTA Photococatalyst[a]**

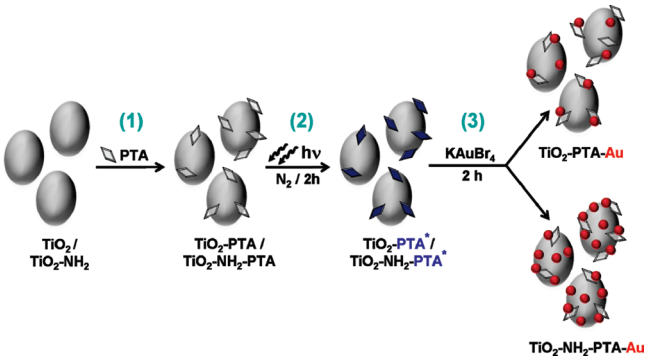


[a] The process involves the functionalization of the surface of pristine and amine-modified $TiO_2$ particles with PTA $[(PW_{12}O_{40})^{3-}]$ ions (step 1), followed by UV irradiation of $TiO_2$−PTA for 2 h, which results in the reduction of $TiO_2$ surface-bound PTA to $[(PW_{12}O_{40})^{4-}]$ ions (step 2). The reduced PTA $[(PW_{12}O_{40})^{4-}]$ ions are indicated as PTA*, which reflects that $TiO_2$-bound PTA is in the excited state and is ready to reduce $AuBr_4^-$ directly on the surface of $TiO_2$−PTA and $TiO_2$−$NH_2$−PTA in the form of $Au^0$ nanoparticles (step 3). The higher loading of Au nanoparticles in $TiO_2$−$NH_2$−PTA−Au in comparison with that in the $TiO_2$−PTA−Au composite is also notable, which is due to more binding of PTA to the amine-functionalized $TiO_2$ surface. Please note that amine has been represented as $NH_2$ for simplicity, which is in the protonated $NH_3^+$ form.

## RESULTS AND DISCUSSION

Scheme 1 summarizes the series of reactions employed for the formation of $TiO_2$−PTA−Au and $TiO_2$−$NH_2$−PTA−Au cocatalysts, illustrating that in step 1 commercially obtained $TiO_2$ and amine-modified titania particles ($TiO_2$−$NH_2$) are functionalized with PTA $[(PW_{12}O_{40})^{3-}]$ ions, resulting in $TiO_2$−PTA and $TiO_2$−$NH_2$−PTA particles. Step 2 involves exposing $TiO_2$−PTA and $TiO_2$−$NH_2$−PTA to UV irradiation for 2 h in the presence of propan-2-ol under a $N_2$ environment. Because PTA is a UV-switchable reducing agent, step 2 leads to the reduction of $(PW_{12}O_{40})^{3-}$ ions bound to the $TiO_2$ surface to $(PW_{12}O_{40})^{4-}$ ions (represented as PTA*). The reduction of PTA molecules upon UV irradiation results in the change in the solution color from milky white to purplish blue, which is a signature of the reduced state of PTA.[31] In the next stage (step 3), when $KAuBr_4$ is added to the UV-excited solutions and solutions are allowed to mature for 2 h, the reduced PTA bound to the $TiO_2$ surface acts as a highly localized reducing agent to reduce $AuBr_4^-$ ions to $Au^0$ nanoparticles directly onto the $TiO_2$ surface. This changes the solution color from blue to pink, indicating the formation of Au nanoparticles and the reoxidation of PTA to $(PW_{12}O_{40})^{3-}$ ions, thereby forming $TiO_2$−PTA−Au and $TiO_2$−$NH_2$−PTA−Au composites. A particularly notable advantage of the proposed approach is that it does not result in the formation of free Au nanoparticles in solution. Advantageously, in our approach, PTA acts as a highly localized reducing agent that forms Au nanoparticles


dx.doi.org/10.1021/la2007765 |Langmuir 2011, 27, 6661–6667

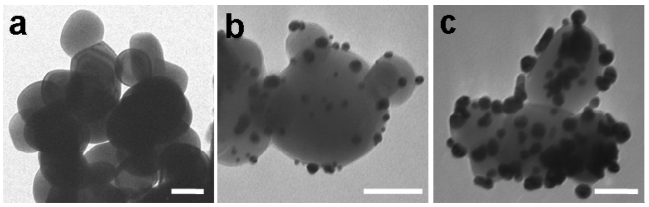


**Figure 1.** TEM micrographs of (a) $TiO_2$, (b) $TiO_2$−PTA−Au, and (c) $TiO_2$−$NH_2$−PTA−Au composites. Scale bars correspond to 100 nm.

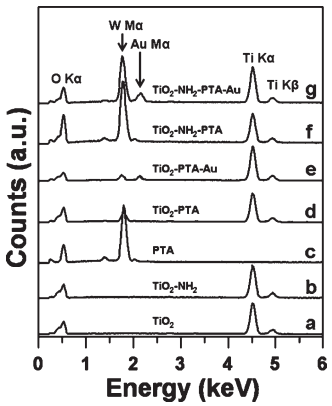


**Figure 2.** EDX analysis of (a) $TiO_2$, (b) $TiO_2$−$NH_2$, (c) PTA, (d) $TiO_2$−PTA, (e) $TiO_2$−PTA−Au, (f) $TiO_2$−$NH_2$−PTA, and (g) $TiO_2$−$NH_2$−PTA−Au. Energy edges characteristic of Ti Kα and Ti K$\beta$ are observed at 4.5 and 4.9 keV, respectively, whereas Ti Lα is present as a shoulder on the O Kα signal at 0.9 keV. Peaks characteristic of W Mα are observed at 1.7 keV in all samples containing PTA, and a Au Mα signal is observed at ca. 2.1 keV. The intensities of all of the spectra, except that of pristine PTA, have been normalized against the Ti Kα signal for comparison.

directly and only onto the $TiO_2$ surface, thus avoiding potential contamination of the solutions with metal nanoparticles.

Figure 1a shows the TEM image of commercially obtained anatase $TiO_2$ after the dispersion in water, which indicates that as-obtained $TiO_2$ powder consisted of 50−200 nm particles of irregular quasi-spherical morphology. When the $TiO_2$ surface was modified with amine or PTA, no apparent change in particle size or morphology was observed under TEM (data not shown for brevity). Moreover, the binding of PTA to $TiO_2$ and $TiO_2$−$NH_2$ was confirmed by EDX spectroscopy, which showed a distinct energy edge at 1.7 keV corresponding to the W Mα line, thus affirming the successful functionalization of $TiO_2$ and $TiO_2$−$NH_2$ with PTA (Figure 2). Interestingly, EDX indicated a significantly higher binding of PTA to $TiO_2$−$NH_2$ (curve f) in comparison with pristine $TiO_2$ (curve d), which is evident from the Ti/W peak ratios in these two samples, wherein the W peak is of a significantly higher intensity in the former. This is expected because since the pristine $TiO_2$ surface is negatively charged as a result of the hydroxyl groups, the negatively charged PTA molecules can bind to the $TiO_2$ surface only through nonspecific interactions. Conversely, amine modification of $TiO_2$ provides a positively charged surface[38,39] that facilitates the strong electrostatic binding of negatively charged PTA to $TiO_2$−$NH_2$. The positively charged surface of $TiO_2$−$NH_2$ was confirmed using zeta potential measurements that revealed a shift in the surface charge of pristine $TiO_2$ particles from −20.3 to +6.7 mV after their amine

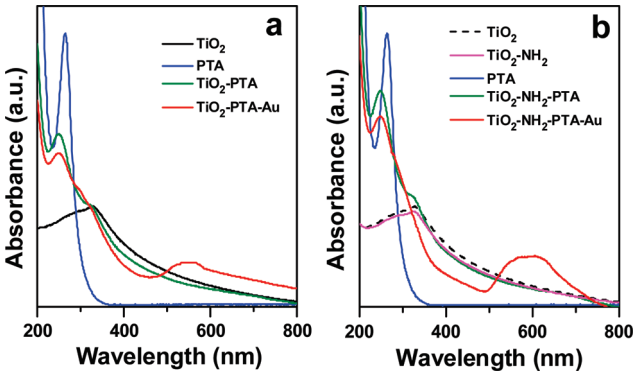


**Figure 3.** UV−visible spectra of (a) $TiO_2$−PTA−Au and (b) $TiO_2$−$NH_2$−PTA−Au composite systems.

functionalization. It should also be noted that to avoid the complicated nomenclature of composites, amine has been represented as $NH_2$ throughout the article, which is in the protonated $NH_3^+$ form. After PTA binding, both $TiO_2$−PTA and $TiO_2$−$NH_2$−PTA composites were found to be negatively charged, as revealed by their zeta potential values of −18.1 and −16.6 eV, respectively. The strong binding of PTA to $TiO_2$−$NH_2$ is further reflected in the comparison of the TEM images of $TiO_2$−PTA−Au (Figure 1b) and $TiO_2$−$NH_2$−PTA−Au (Figure 1c), which show significantly higher loadings of Au nanoparticles on amine-modified $TiO_2$. Because more PTA is present in $TiO_2$−$NH_2$−PTA in comparison with that in $TiO_2$−PTA and because PTA acts as a highly localized reducing agent, a higher surface coverage of $TiO_2$−$NH_2$−PTA−Au results via more reduction of $AuBr_4^-$ ions to Au nanoparticles onto the $TiO_2$ surface. The Au nanoparticles formed in the $TiO_2$−PTA−Au composite were found to be well-dispersed, quasi-spherical, and 2−10 nm in diameter (Figure 1b), whereas those in the $TiO_2$−$NH_2$−PTA−Au composite were found to be clustered at several places, varied in shape from quasi-spherical to irregular, and ranging in size from 5 to 30 nm (Figure 1c). The EDX analysis further confirmed the presence of Au in these samples, and more so, a higher intensity of Au signatures corresponding to a Au Mα energy edge at 2.1 keV was observed in $TiO_2$−$NH_2$−PTA−Au (curve g, Figure 2) than in the $TiO_2$−PTA−Au composite (curve e, Figure 2). Additionally, large-area TEM scans of $TiO_2$−PTA−Au and $TiO_2$−$NH_2$−PTA−Au composites did not reveal the formation of any free Au nanoparticles, thus affirming that PTA acts as a localized reducing agent on the surface of $TiO_2$. Both TEM and EDX analysis therefore clearly confirm that the amine modification of $TiO_2$ particles enables a higher loading of PTA molecules on its surface, which further facilitates a higher degree of Au nanoparticle formation on amine-modified surfaces.

The formation of the aforementioned composite materials was further monitored using UV−visible spectroscopy, as is shown for $TiO_2$−PTA−Au and $TiO_2$−$NH_2$−PTA−Au composites, respectively, in Figure 3a,b. The anatase $TiO_2$ used in this study showed an absorbance maximum at ca. 325 nm, which does not change significantly after its amine functionalization ($TiO_2$−$NH_2$). PTA molecules showed a sharp feature at ca. 263 nm that corresponds to absorption by its Keggin structure (blue curves).[31] When PTA is bound to $TiO_2$ or $TiO_2$−$NH_2$, the absorbance characteristic of the Keggin structure of PTA is observed to blue shift to ca. 250 nm, indicating an interaction between PTA and the surfaces of the $TiO_2$ particles (green curves). Interestingly,


dx.doi.org/10.1021/la2007765 |*Langmuir* 2011, 27, 6661–6667

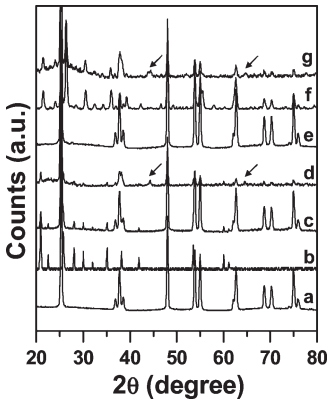


**Figure 4.** XRD patterns of (a) $TiO_2$, (b) PTA, (c) $TiO_2$−PTA, (d) $TiO_2$−PTA−Au, (e) $TiO_2$−$NH_2$, (f) $TiO_2$−$NH_2$−PTA, and (g) $TiO_2$−$NH_2$−PTA−Au. The arrows correspond to peaks attributable to face-centered-cubic (fcc) gold.

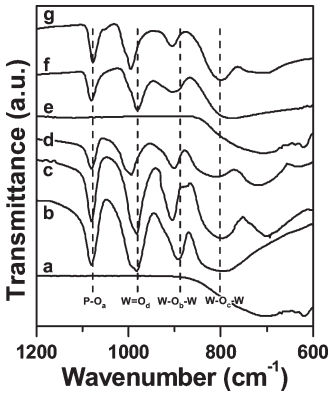


**Figure 5.** FTIR spectra of (a) $TiO_2$, (b) PTA, (c) $TiO_2$−PTA, (d) $TiO_2$−PTA−Au, (e) $TiO_2$−$NH_2$, (f) $TiO_2$−$NH_2$−PTA, and (g) $TiO_2$−$NH_2$−PTA−Au.

for the same concentration of $TiO_2$ particles, the peak intensity corresponding to PTA was found to be greater in the $TiO_2$−$NH_2$−PTA system than in the $TiO_2$−PTA system (green curves). This can be attributed to the higher loading of negatively charged PTA molecules onto positively charged amine-modified $TiO_2$ particles via strong electrostatic interactions, as was also evident from EDX analysis (Figure 2). Furthermore, the UV−vis spectra of $TiO_2$−PTA−Au and $TiO_2$−$NH_2$−PTA−Au composites showed broad surface plasmon resonance (SPR) features between 500 and 600 nm (red curves) with peak maxima at ca. 550 and 600 nm, respectively. Gold nanoparticles dispersed in an aqueous environment typically exhibit SPR features at ca. 520 nm (for 10−20 nm particles), which is known to be shifted according to the surrounding dielectric environment.[40] The observed red shifts in these samples, corresponding to Au SPR, can be attributed to the close proximity of Au nanoparticles to the $TiO_2$−PTA surface, which can alter the Au SPR feature because of the change in the dielectric property of the environment. Additionally, the broadness of the Au SPR feature in the $TiO_2$−$NH_2$−PTA−Au composite can be partially attributed to the clustering of Au nanoparticles onto the $TiO_2$ surface, as was also observed using TEM (Figure 1c).

The change in crystallinity of the synthesized composites was further monitored using XRD (Figure 4). XRD patterns a and b in Figure 4 correspond to pristine $TiO_2$ and PTA, respectively, clearly showing well-defined diffraction peaks attributable to the anatase phase of $TiO_2$ (JCPDS 01-070-6826) and pure PTA (JCPDS 00-050-0662). When PTA is bound to the $TiO_2$ surface ($TiO_2$−PTA), most of the signals corresponding to anatase $TiO_2$ along with few PTA signatures can be seen (pattern c); however, for $TiO_2$−PTA, the intensity of PTA peaks are observed to decrease dramatically in intensity, which is most likely due to PTA forming only a thin coating on the $TiO_2$ surface and thus the majority of the observed signals are due to the crystal phases of anatase $TiO_2$. In the Au-decorated $TiO_2$−PTA sample, additional peaks corresponding to the [200] and [220] facets of face-centered-cubic (fcc) gold are observed at ca. 44 and ca. 65° 2$\theta$, respectively (pattern d, marked with arrows), with a further reduction in the intensity of the XRD peaks corresponding to PTA and $TiO_2$. Amine modification of the $TiO_2$ surface ($TiO_2$−$NH_2$, pattern e) produces a pattern identical to that of pure $TiO_2$, confirming that the amine modification has no effect on the crystalline properties of the $TiO_2$ lattice. Unlike the $TiO_2$−PTA composite (pattern c), the XRD pattern of the $TiO_2$−$NH_2$−PTA composite contains intense peaks attributable to PTA (pattern f), which once again suggests that a relatively higher amount of PTA is present on the surface of the $TiO_2$−$NH_2$−PTA compared to that on $TiO_2$−PTA, which correlates well with the EDX results. Furthermore, the XRD pattern corresponding to the $TiO_2$−$NH_2$−PTA−Au composite shows signatures corresponding to $TiO_2$, PTA, and fcc gold, confirming the presence of all of the respective components in this composite (pattern g).

Information regarding the mode of binding of PTA molecules to $TiO_2$ and Au nanoparticles was obtained using FTIR spectroscopy (Figure 5). It is well known that the Keggin structure of PTA ($H_3PW_{12}O_{40}$) consists of a cage of tungsten atoms linked by oxygen atoms with the phosphorus atom at the center of the tetrahedra.[41,42] Oxygen atoms form four physically distinct bonds (P−$O_a$, W−$O_b$−O, W−$O_c$−W, and W=$O_d$) within the Keggin structure, which have distinct infrared signatures. P−$O_a$ corresponds to an asymmetric stretching vibrational mode between phosphorus and oxygen atoms at the center of the Keggin structure, giving rise to a characteristic signature at 1080 $cm^{-1}$. W−$O_b$−O and W−$O_c$−W correspond to bending vibrational modes of oxygen atoms, which form a bridge between the two tungsten atoms within the Keggin structure. Among these two, W−$O_b$−W represents the oxygen atoms at the corners of the Keggin structure and W−$O_c$−W represents the oxygen atoms along the edges, giving rise to characteristic vibrational modes at 890 and 800 $cm^{-1}$ for W−$O_b$−W and W−$O_c$−W respectively. The fourth vibrational mode, W=$O_d$, corresponds to the asymmetric stretching of terminal oxygen atoms reflected at 980 $cm^{-1}$.[41,42] It is evident from the FTIR spectra that $TiO_2$ (curve a, Figure 5) and $TiO_2$−$NH_2$ (curve e) do not show significant features at wavenumbers of more than 800 $cm^{-1}$, whereas PTA (curve b) shows four characteristic absorbance bands attributable to P−$O_a$, W=$O_d$, W−$O_b$−W, and W−$O_c$−W at 1080, 980, 890, and 800 $cm^{-1}$, respectively. Therefore, shifts in the vibrational modes of oxygen atoms in the PTA molecule after its binding to $TiO_2$ can be easily followed using FTIR spectroscopy. Upon complexation of PTA to the $TiO_2$ surface (curve c), a remarkable shift in the W−$O_b$−W bending vibrations from ca. 890 to ca. 905 $cm^{-1}$ is observed, without any noticeable shift in other vibrational modes. The significant blue shift of 15 $cm^{-1}$ in the W−$O_b$−W bending


dx.doi.org/10.1021/la2007765 |*Langmuir* 2011, 27, 6661–6667

vibrational mode of PTA suggests that PTA interacts quite strongly with the $TiO_2$ surface and binds to $TiO_2$ through the oxygen atoms at the corners of the Keggin structure ($W-O_b-W$). Once Au nanoparticles are reduced onto the $TiO_2-PTA$ surface, this does not lead to further shifts in the $W-O_b-W$ mode; however, it is accompanied by a blue shift of the symmetric stretching vibrations of terminal oxygen atoms ($W=O_d$) from the original 980 $cm^{-1}$ (in free PTA) to 995 $cm^{-1}$ (in $TiO_2-PTA-Au$) (curve d). This suggests that Au nanoparticles binding to the Keggin structure occurs through terminal oxygen atoms. Amine-modified $TiO_2$ shows similar behavior toward PTA binding, such as that observed for pristine $TiO_2$, indicating that PTA may also bind to the $NH_2$ functional groups through oxygen atoms at the corners of the Keggin structure (curve f), followed by binding to Au through its terminal oxygen atoms (curve g). The strong binding of PTA molecules to the nanocomposites prepared in this study further indicates that these nanocomposites might be suitable for solution-based photocatalysis applications, without causing significant leaching of $TiO_2$-bound PTA during application.

As previously discussed, $TiO_2$ is probably one of the most investigated materials for its photocatalytic properties. However, it is also well known that in the majority of the wide-band-gap semiconductor materials including $TiO_2$ a major rate-limiting factor determining their photocatalytic performance is the undesirable process of electron/hole recombination.[43] In this process, as electrons are promoted from the valence band across the band gap into the conduction band, there exists a very large driving force to recombine the electron and the newly generated hole.[43] By controllably depositing metal nanoparticles onto the surface of $TiO_2$ particles, a Schottky barrier can be created at the metal–semiconductor junction,[44] which is due to the difference in the Fermi-level positions of the metal and the semiconductor.[45] This leads to a continuous transfer of electrons from $TiO_2$ to metal nanoparticles until the equilibrium of the Fermi energy levels is achieved. In such metal–metal oxide systems, during photoexcitation, electrons can migrate from the semiconductor to the metal across the Schottky barrier, where they are trapped and the electron/hole recombination phenomena are suppressed, whereby the hole is then free to diffuse through $TiO_2$ to the surface where it can be used to oxidize organic species.[43] Therefore, metal nanoparticles deposited on the $TiO_2$ surface can play an important role in catalyzing the interfacial charge-transfer process,[46,47] which may result in a significant improvement in the photochemical performance of the material, as demonstrated previously.[45,48]

Because in our current study PTA has been used as an intermediate layer between $TiO_2$ and Au nanoparticles and PTA molecules are well-known for their outstanding electron-transfer ability,[31] we investigated the photocatalytic performance of our materials toward the degradation of an organic material, azo dye Congo red (CR) in the presence of a simulated solar spectrum for 30 min. Being an organic dye, CR degradation during photoexcitation in the presence of nanocomposites could be easily followed using UV–vis spectroscopy (Figure 6). In a control experiment, when CR was exposed to simulated solar light in the absence of any photocatalyst, this led to only ca. 7% degradation of the dye (as determined by the reduction in the $A_{500}$ of CR). As expected, the presence of anatase $TiO_2$ led to an increase in the photodegradation of CR to ca. 20%, indicating that unmodified $TiO_2$ was photoactive and had the ability to facilitate the degradation of CR. Similarly, an equivalent amount of amine-modified titania ($TiO_2-NH_2$) showed similar photoactivity, resulting in ca. 23% degradation of

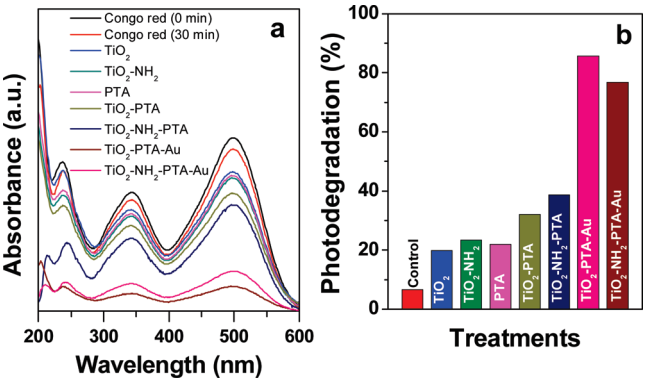


**Figure 6.** (a) UV–visible spectra of Congo red dye upon exposure to a range of photocatalysts for 30 min under simulated solar light conditions. (b) Percent photodegradation of Congo red expressed as a reduction in the intensity of absorbance at 500 nm. The control in part b represents the % photodegradation of Congo red in the absence of a photocatalyst but in the presence of simulated solar light for 30 min.

the dye molecules, suggesting that the amine modification of $TiO_2$ does not significantly alter its photocatalytic performance. Notably, pristine PTA is also known for its photocatalytic properties,[37] which resulted in photoactivity similar to that of $TiO_2$ and $TiO_2-NH_2$ at ca. 22%. Conversely, after PTA binding, $TiO_2-PTA$ and $TiO_2-NH_2-PTA$ led to an increased photoactivity, resulting in ca. 32 and 39% degradation of CR, respectively. This increase in photocatalytic performance can be attributed to the cocatalytic activity of these composites as a result of the presence of both $TiO_2$ and PTA molecules. Marginally higher photocatalytic activity of $TiO_2-NH_2-PTA$ in comparison with that of $TiO_2-PTA$ can be assigned to the higher loading of PTA in the former for equivalent amounts of $TiO_2$ used. Notably, introducing Au into the composite material to form $TiO_2-PTA-Au$ and $TiO_2-NH_2-PTA-Au$ cocatalysts resulted in a dramatic improvement in the photocatalytic performance, leading to ca. 86 and 77% degradation of CR, respectively. It is interesting that although $TiO_2-NH_2-PTA$ showed marginally better performance than $TiO_2-PTA$, the trends were reversed when Au was added to these materials (i.e., $TiO_2-PTA-Au$ was found to perform better than $TiO_2-NH_2-PTA-Au$). From TEM, EDX, and XRD analyses, it is clearly evident that the number and size of Au nanoparticles decorating the amine-modified $TiO_2$ surface are significantly larger than those of the unmodified surface. The reduced photoactivity of $TiO_2-NH_2-PTA-Au$ may be partially attributable to relatively higher Au loading in this system, which might decrease the total effective $TiO_2$ surface area during the photocatalytic degradation of CR. Because the redox activity of Au nanoparticles by readily accepting electrons from a suitable donor ($TiO_2$) can be size-dependent, it is also likely that the presence of relatively larger clustered Au nanoparticles in the $TiO_2-NH_2-PTA-Au$ composite may reduce its photoactivity compared to that of the $TiO_2-PTA-Au$ composite, the latter of which showed well-segregated, smaller Au nanoparticles.

Additional control experiments were performed to ascertain that $TiO_2-PTA-Au$ and $TiO_2-NH_2-PTA-Au$ composites indeed act as cocatalysts, wherein $TiO_2$, PTA, and Au play some role in enhancing the photocatalytic activity. In these control experiments, Au nanoparticles were directly photodeposited onto pristine and amine-modified titania without utilizing PTA


dx.doi.org/10.1021/la2007765 |*Langmuir* 2011, 27, 6661–6667

as the intermediate layer, thereby leading to $TiO_2$—Au and $TiO_2$—$NH_2$—Au composites, respectively (TEM in Supporting Information, Figure S1). In comparison to composites that had all three components ($TiO_2$, PTA, and Au; 77—86% activity), the composites without PTA ($TiO_2$—Au and $TiO_2$—$NH_2$—Au) showed only 51—54% photocatalytic activity (Supporting Information, Figure S2). These experiments clearly show that the presence of PTA as a photoactive linker molecule can have a significant influence on increasing the overall photocatalytic ability of $TiO_2$-based systems. Because FTIR spectroscopy showed strong interactions of PTA sandwiched between $TiO_2$ and Au with both of these systems, we believe that in addition to the photocatalytic activity of PTA molecules an intermediate PTA layer between semiconductor and metal may provide an additional driving force for facilitating charge transfer between $TiO_2$ and Au as a result of the strong electron transferability of PTA molecules. This can result in a dramatic increase in the photocatalytic performance of nanocomposites, as is evident from this study that shows a 2.7-fold increase in the photoactivity of anatase $TiO_2$ after adding Au to it ($TiO_2$ 20% vs $TiO_2$—Au 54%) and a 4.3-fold increase after introducing PTA along with Au to it ($TiO_2$ 20% vs $TiO_2$—PTA—Au 86%).

## CONCLUSIONS

We have demonstrated for the first time the synthesis of a $TiO_2$-based cocatalytic system using PTA both as a photocatalytic linker molecule and a highly localized UV-switchable reducing agent for the decoration of metal nanoparticles on the surface of anatase $TiO_2$ particles. The study shows that the presence of both Au nanoparticles and PTA in a cocatalytic system on the $TiO_2$ surface, as opposed to a $TiO_2$ surface decorated directly with metal nanoparticles, can have a dramatic effect on increasing the photocatalytic performance of the composite system. The generalized localized reduction approach for preparing $TiO_2$—Keggin—metal cocatalysts reported here can be equally extended to similar systems. Our further investigations will explore the relative efficiency of different metal nanoparticles (Au, Ag, Pt, and Cu) and a range of Keggin-type polyoxometallates toward increasing the photocatalytic performance of titania-based systems. Because of the unique electron-transfer ability of polyoxometallates, some of these systems might prove useful in solar cell applications.

## METHODS

**Materials.** Potassium tetrabromoaurate dihydrate ($KAuBr_4 \cdot 2H_2O$) and 3-aminopropyltriethoxysilane (APTES) were obtained from Sigma-Aldrich, anatase titanium dioxide ($TiO_2$) powder was obtained from BDH Chemicals, 12-phosphotungsticacid hydrate ($H_3PW_{12}O_{40} \cdot 2H_2O$) was obtained from Scharlau Chemie, and ammonia (28%) was obtained from Ajax Fine Chemicals. All chemicals were used as received without any modification.

**Amine Modification of $TiO_2$.** Anatase $TiO_2$ powder (100 mg) was added to a solution containing 20 mL of ethanol, 1 mL of ammonia (28%), and 4 mL of APTES. The suspension was left overnight under mechanical stirring to prevent the $TiO_2$ powder from settling. The suspension was then centrifuged, the supernatant was removed, and the solid material was washed three times with deionized water (Milli-Q). The amine-modified $TiO_2$ was then dispersed in 25 mL of deionized water, stored for later use at room temperature, and is designated as $TiO_2$—$NH_2$ in subsequent experiments.

**PTA Functionalization of $TiO_2$ and $TiO_2$—$NH_2$.** In two parallel experiments, 100 mg each of $TiO_2$ and $TiO_2$—$NH_2$ powders were separately immersed in 100 mL of a 10 mM PTA solution and left overnight under mechanical stirring. The solid products were centrifuged and washed three times with deionized water to facilitate the removal of uncoordinated PTA molecules. The composites were then dispersed in 25 mL of deionized water, which resulted in two products corresponding to $TiO_2$—PTA and $TiO_2$—$NH_2$—PTA wherein PTA molecules were bound to the $TiO_2$ surface, either directly or through an amine linkage, respectively.

**Photochemical Deposition of Au Nanoparticles onto $TiO_2$—PTA and $TiO_2$—$NH_2$—PTA.** The strong UV-switchable reduction capability of PTA molecules bound to $TiO_2$ particles was utilized for the reduction of $AuBr_4^-$ ions onto the $TiO_2$ surface. In two parallel experiments in quartz tubes, 4 mL each of $TiO_2$—PTA (4 mg $mL^{-1}$) and $TiO_2$—$NH_2$—PTA (4 mg $mL^{-1}$) solutions were mixed with 1 mL of propan-2-ol in quartz tubes, followed by purging with nitrogen gas for 15 min and photoexciting solutions under a UV lamp (excitation wavelength 260 nm) for 2 h to allow $TiO_2$-bound PTA molecules to be reduced. To each of these solutions, 5 mL of 1 mM $KAuBr_4 \cdot 2H_2O$ was added and allowed to mature for 2 h. After 2 h, the suspensions were centrifuged at 3000 rpm to precipitate $TiO_2$—PTA—Au (light pink in color) and $TiO_2$—$NH_2$—PTA—Au (darker purplish red in color) composites. The resultant composites were resuspended in 25 mL of deionized water and stored at room temperature.

**Material Characterization.** All the aforementioned materials were examined at various stages of synthesis using transmission electron microscopy (TEM), UV—visible spectroscopy (UV—vis), energy-dispersive X-ray (EDX) and Fourier transform infrared (FTIR) spectroscopy, X-ray diffraction (XRD), and zeta potential measurements. The samples for TEM were prepared by drop coating the solution onto a carbon-coated copper grid, followed by TEM measurements using a JEOL 1010 instrument operated at an accelerating voltage of 100 kV. UV—visible absorbance analysis was performed using a Cary 50 biospectrophotometer at a spectral resolution of 1 nm, EDX analysis was performed using an FEI NovaSEM instrument coupled with an EDX Si(Li) X-ray detector, FTIR spectroscopy was performed using Perkin-Elmer Spectrum 100 instrument, and XRD was performed using a Bruker AXS D8 Discover with a general area detector diffraction system. Zeta potential measurements were performed in Milli-Q water using a Malvern 2000 Zetasizer.

**Photocatalytic Degradation of an Organic Dye.** The photocatalytic ability of $TiO_2$-based composites was studied by adding composite material to an aqueous solution of organic azo dye Congo red (CR) and recording the intensity of the characteristic absorption maxima after a period of 30 min of exposure to simulated solar light. To assess the photocatalytic performance, nanocomposites containing 12 mg equiv of $TiO_2$ were separately added to 10 mL aqueous solutions containing 10 $\mu$M Congo red. In a control experiment involving pristine PTA, the amount of PTA used during photocatalysis experiments corresponds to the equivalent amount that was used to bind PTA to $TiO_2$ and $TiO_2$—$NH_2$. Please note that not the entire amount of PTA used in the binding experiment was bound to $TiO_2$ and $TiO_2$—$NH_2$; therefore, a significantly larger amount of PTA has been used in the control photocatalysis experiment. For photocatalysis measurements, an Abet Technologies LS-150 series 150W Xe arc lamp source that simulates solar light under equator conditions was used, with the sample placed in a quartz vial 10 cm from the source under mechanical stirring. After 30 min of irradiation, the samples were centrifuged to remove the composite material, and the remaining solutions were examined by UV—vis spectroscopy.

## ASSOCIATED CONTENT

**Supporting Information.** TEM images of $TiO_2$—Au and $TiO_2$—$NH_2$—Au composites and photodegradation of Congo red in the presence of $TiO_2$—Au and $TiO_2$—$NH_2$—Au composites. This material is available free of charge via the Internet at http://pubs.acs.org.

## AUTHOR INFORMATION

**Corresponding Author**

*(S.K.B.) E-mail: suresh.bhargava@rmit.edu.au. (V.B.) E-mail: vipul.bansal@rmit.edu.au. Phone: +61 3 9925 2121. Fax: +61 3 9925 3747.

## ACKNOWLEDGMENT

V.B. acknowledges the Australian Research Council (ARC), Commonwealth of Australia, for the award of an APD fellowship and research support through the ARC Discovery (DP0988099; DP110105125), Linkage (LP100200859), and LIEF (LE0989615) grant schemes. The support to V.B. by RMIT University through the award of seed grants, incentive capital funding, and an emerging researcher grant is also acknowledged. V.B. also acknowledges the support of the Ian Potter Foundation to establish a multi-mode spectrophotometry facility at RMIT University, which was used in this study.

## REFERENCES

(1) Satterfield, C. N. *Heterogeneous Catalysis in Industrial Practice*, 2nd ed.; McGraw-Hill: New York, 1991.
(2) del Arco, M.; Caballero, A.; Malet, P.; Rives, V. *J. Catal.* **1988**, 120–128.
(3) Lached, H.; Puzenat, E.; Houas, A.; Ksibi, M.; Elaloui, E.; Guillard, C.; Herrmann, J. *Appl. Catal.* **2002**, 75–90.
(4) Sharma, S. D.; Saini, K. K.; Kant, C.; Sharma, C. P.; Jain, S. C. *Appl. Cataly., B* **2008**, 233–240.
(5) Mahmoodi, N. M.; Arami, M.; Limaee, N. Y.; Gharanjig, K. *J. Hazard. Mater.* **2007**, 65–71.
(6) Barraud, E.; Bosc, F.; Edwards, D.; Keller, N.; Keller, V. *J. Catal.* **2005**, 318–326.
(7) Hagfeldt, A.; Gratzel, M. *Acc. Chem. Res.* **2000**, 269–277.
(8) Anpo, M. *Catal. Surv. Jpn.* **1997**, 169–179.
(9) Baker, D. R.; Kamat, P. V. *Adv. Funct. Mater.* **2009**, 805–811.
(10) Kikuchi, H.; Kitano, M.; Takeuchi, M.; Matsuoka, M.; Anpo, M.; Kamat, P. V. *J. Phys. Chem. B* **2006**, 5537–5541.
(11) Wilke, K.; Breuer, H. D. *J. Photochem. Photobiol., A* **1998**, 49–53.
(12) Bouras, P.; Stathatos, E.; Lianos, P. *Appl. Catal.* **2006**, 51–59.
(13) Heller, A.; Degani, Y.; Johnson, D. W. J.; Gallagher, P. K. *Proc. Electrochem. Soc.* **1988**, 23–33.
(14) Kudo, A.; Domen, K.; Maruya, K.; Onishi, T. *Bull. Chem. Soc. Jpn.* **1988**, 1535–1538.
(15) Nosaka, Y.; Norimatsu, K.; Miyama, H. *Chem. Phys. Lett.* **1984**, *106*, 128–131.
(16) Kamat, P. V.; Shanghavi, B. *J. Phys. Chem. B* **1997**, *101*, 7675–7679.
(17) Doron, A.; Katz, E.; Willner, I. *Langmuir* **1995**, 1313–1317.
(18) Colvin, V. L.; Goldstein, A. N.; Alivisatos, A. P. *J. Am. Chem. Soc.* **1992**, 5221–5230.
(19) Yonezawa, T.; Matsune, H.; Kunitake, T. *Chem. Mater.* **1999**, 33–35.
(20) Vittadini, A.; Selloni, A. *J. Chem. Phys.* **2002**, 353–361.
(21) Cattaruzza, E. *Nucl. Instrum. Methods Phys. Res., Sect. B* **2000**, 141–155.
(22) Deki, S.; Aoi, Y.; Yanagimoto, H.; Ishii, K.; Akamatsu, K.; Mizuhata, M.; Kajinami, A. *J. Mater. Chem.* **1996**, 1879–1882.
(23) Maruyama, O.; Senda, Y.; Omi, S. *J. Non-Cryst. Solids* **1999**, 100–106.
(24) Chandrasekharan, N.; Kamat, P. V. *J. Phys. Chem. B* **2000**, 10851–10857.
(25) Sambi, M.; Pin, E.; Sangiovanni, G.; Zaratin, L.; Granozzi, G.; Parmigiani, F. *Surf. Sci.* **1996**, 169–173.
(26) Datye, A. K.; Kalakkad, D. S.; Yao, M. H.; Smith, D. J. *J. Catal.* **1995**, 148–153.
(27) Sault, A. G.; Peden, C. H.; Boespflug, E. P. *J. Phys. Chem.* **1994**, 1652–1662.
(28) Bernal, S.; Botana, F. J.; Calvino, J. J.; Lopez, C.; Perez-Omil, J. A.; Rodriguez-Izquierdo, J. M *J. Chem. Soc., Faraday Trans.* **1996**, 2799–2809.
(29) Che, M.; Bennett, C. O. *Adv. Catal.* **1989**, 55–172.
(30) Pope, M. T.; Mueller, A. *Angew. Chem., Int. Ed.* **1991**, 34–48.
(31) Mandal, S.; Selvakannan, P.; Pasricha, R.; Sastry, M. *J. Am. Chem. Soc.* **2003**, 8440–8441.
(32) Mizuno, N.; Watanabe, T.; Mizuno, N. *J. Phys. Chem.* **1985**, 80–85.
(33) Lee, K. Y.; Arai, T.; Nakata, S.; Asaoka, S.; Okuhara, T.; Misono, M. *J. Am. Chem. Soc.* **1992**, 2836–2842.
(34) Fogg, A. G.; Bsebsu, N. K.; Birch, B. J. *Talanta* **1981**, 78.
(35) Tell, B. *J. Electrochem. Soc.* **1980**, *127*, 2451–2454.
(36) Mandal, S.; Anandrao, B. M.; Sastry, M. *J. Mater. Chem.* **2004**, 2868–2871.
(37) Papaconstantinou, E. *Chem. Soc. Rev.* **1989**, *18*, 1.
(38) Muller, C. A.; Schneider, M.; Mallat, T.; Baiker, A. *Appl. Catal., A* **2004**, 253–261.
(39) Yang, Y.; Guo, Y.; Hu, C.; Wang, Y.; Wang, E. *Appl. Catal., A* **2004**, 201–210.
(40) Grzelczak, M.; Perez-Juste, J.; Mulvaney, P.; Liz-Marzan, L. M. *Chem. Soc. Rev.* **2008**, *37*, 1783–1791.
(41) Kumbar, S. M.; Hallidugdi, S. B. *Catal. Commun.* **2007**, 800.
(42) Sanyal, A.; Mandal, S.; Sastry, M. *Adv. Funct. Mater.* **2005**, 273.
(43) Linsebigler, A. L.; Lu, G.; John T. Yates, J. *Chem. Rev.* **1995**, 735–758.
(44) Iliev, V.; Tomova, D.; Bilyarska, G.; Tyuliev, G. *J. Mol. Catal. A: Chem.* **2007**, 32–38.
(45) Jakob, M.; Levanon, H.; Kamat, P. V. *Nano Lett.* **2003**, *3*, 353–358.
(46) Kamat, P. V. *J. Phys. Chem. B* **2002**, *106*, 7729.
(47) Subramanian, V.; Wolf, E. E.; Kamat, P. V. *Langmuir* **2003**, *19*, 469.
(48) Subramanian, V.; Wolf, E.; Kamat, P. V. *J. Phys. Chem. B* **2001**, *105*, 11439.